The Nucleus, **46** (4) 2009 : 479-485

The Nucleus
A Quarterly Scientific Journal of Pakistan
Atomic Energy Commission
NCLEAM, ISSN 0029-5698

SYNTHESIS OF TRANSITION METAL OXIDE NANOCRYSTALS BY COST EFFECTIVE HYDROTHERMAL PROCESS

Y. KHAN, *S. K. DURRANI[1], M. R. KHAN[2] and M. A. HAQ[3]

Department of Chemical and Materials Engineering, PIEAS, P. O. Nilore, Islamabad, Pakistan

[1]Materials Division, Directorate of Technology, PINSTECH, P. O. Nilore, Islamabad, Pakistan

[2]Centralized Resource Laboratory, Department of Physics, University of Peshawar, Peshawar, Pakistan

[3]Physics Division, Directorate of Science, PINSTECH, P.O. Nilore, Islamabad, Pakistan

(Received November 04, 2009 and accepted in revised form November 26, 2009)

Simple and cost effective hydrothermal process was used for synthesis of nanocrystals of transition metal oxides such as manganese oxide (α-MnO_2), nickel oxide (NiO) and zinc oxide (ZnO). These nanocrystals were synthesized through hydrothermal decomposition under autogenous pressure condition using metal nitrates and ammonium hydroxide salts in aqueous solutions. The percent yield of synthesized selective oxide products was very good at pH values (> 3.2-3.5 for α-MnO_2 and 9-9.6 for NiO and ZnO) irrespective of the solvent composition. The synthesized products were characterized by X-ray diffraction (XRD), Scanning electron microscopy (SEM), Transmission electron microscopy (TEM) and Brunauer-Emmet-Teller analysis (BET). The XRD results indicated that the synthesized MnO_2, NiO and ZnO had body centered tetragonal, cubic and wurtzite structures having crystalline size 68±0.74, 33±0.14 and 54±0.38 nm respectively. However, the average crystalline sizes derived from BET method were found higher than XRD values indicated the agglomeration of nanocrystals. SEM analysis revealed the thickness of MnO_2 nanowires and NiO nanobelts were in range of 50-90nm and 20-40nm respectively whereas the diameter of ZnO nanorods was about 80-200nm and lengths of over 8-12μm.

Keywords: Nanocrystals, Synthesis, Hydrothermal process, Transition metal oxides

1. Introduction

Any physical substance with structural dimensions between 1-100 nm can be defined as a nanomaterial. Compared with bulk materials, nanocrystalline materials exhibit completely different properties due to their enhanced surface-to-volume ratio and quantum confinement effect [1-2]. Among the nanomaterials, nano metal oxides are essential for the development of smart and efficient devices and systems. These nano oxides exhibit novel optical, electrical properties and are used in the fabrication of microelectronic circuits, sensors, piezoelectric devices, fuel cells, coatings for the passivation of surface against corrosion, and as catalysts [3-4]. The important nano metal oxides are transition metal oxides (TMO) like iron oxide (Fe_3O_4, Fe_2O_3), nickel oxide (NiO), manganese oxide (MnO_2), tin oxide (SnO), titanium dioxide (TiO_2), and zinc oxide (ZnO). As electrode materials for supercapacitors, hydrous ruthenium oxide shows a high capacity of over 700F/g and excellent cyclability in aqueous H_2SO_4 [5]. Because of its high cost, alternative metal oxide electrode materials are being developed to replace ruthenium oxide; e.g. NiO and MnO_2 [6]. MnO_2 has been used as a supercapacitor (pseudocapacitor) because of its abundance in nature, cost and environmental friendliness [7]. NiO has many technological applications due to its electrical, magnetic, catalytic and optical properties [8]. ZnO is a promising material in the field of nanoelectronics and photoelectronic devices because it is a wide band-gap semiconductor [9-10]. As regard with the synthesis of nano oxides wet-chemical methods have been extensively recognized as an efficient approach to prepare these oxides at low temperatures. The most common and widely used wet chemical methods for the preparation of nanoscale transition metal oxides are coprecipitation [11] sol-gel [12], micro-emulsion [13], self-combustion [14], solvothermal

* Corresponding author : durranisk@gmail.com

Table 1. Chemical compositions of raw materials.

Chemicals	Formulae	Purity (%)	Source
Ammonia hydroxide	NH_4OH	35	BDH
Nickel sulphate hexa hydrate	$Ni\ SO_4\ .6H_2\ O$	>98	Fluka
Nitric acid	HNO_3	65	BDH
Sodium hydroxide	NaOH	99.9	Merk
Zinc nitrate hexa hydrate	$Zn\ (NO_3)_2.6H2O$	99.9	Merk
Double Distilled Water (DDW)	H_2O	Carbonate (CO_3^{-2})free	Prepared in Laboratory

Table 2. Hydrothermal reaction conditions for nanocrystals formation of MnO_2, NiO and ZnO.

Specimens	25%NH_4OH (ml)	1MNaOH (ml)	$KClO_3$ (gm)	*Reaction Conditions*		
				pH	Temperature (^oC)	*Time (hrs)*
MnO_2	-	-	1.3	3.2	160	*16*
NiO	15	-	-	9.2	200	*6*
ZnO	-	*7*	-	*9.6*	*180*	*8*

and hydrothermal [15]. These processes have many advantages and disadvantages depending on desired properties and applications. All processes except the hydrothermal are not economical because of using expensive raw materials and unavailability of suitable commercial precursors such as metal alkoxides, surfactant like cetyl-trimethyl-ammonium bromide (CTAB) and emulsifiers like sodium dodecylsulphate (SDC), aerosol bis(2-ethylhexyl) sulfosuccinate (AOT), and pentaethylene glycol dodecyl ether (PEGDE) [16]. Among these synthesis routes, hydrothermal process shows promising potential for the synthesis of nanostructured such as nanorods, nanowires and nanoparticles of transition metal oxides, owing to its high purity, good chemical homogeneity, low calcination temperature, effortless, and cost effective process without involving catalysts or expensive organic precursors and templates. Hydrothermal method represents a soft chemical procedure in one step with lower energy consumption (calcination) and low environmental impact than other synthesis routes [17]. An additional merit of this process is attributed to the low cost for instrumentation, energy and precursors. It allows a good control of microstructure, stoichiometry and properties. In the present work a simple and cost effective hydrothermal route was selected for synthesis of nanosize metal oxides like manganese oxide (MnO_2), nickel oxide (NiO) and zinc oxide (ZnO).

2. Experimental

2.1. Synthesis of nano oxides

All of the raw materials were analytical reagent and used as-received without further purification. The characteristics of raw materials and reaction condition parameters are shown in Tables 1-2. The hydrothermal process for the synthesis of nanocrystals of MnO_2, NiO and ZnO was carried out as described somewhere else [18 -19], In typical synthesis, known amount of metal salts were dissolved into double distilled water (DDW) with vigorous stirring to prepare desired molar solution. Sodium (NaOH) or ammonium hydroxide (NH_4OH) aqueous solution was added dropwise and pH of the suspension was maintained at 8-10 with attached pH-meter (J. P. Selecta 2006, Spain) for nickel and zinc salts solution respectively, whereas potassium chlorate ($KClO_3$) was added to manganese salt solution as an oxidizer. Finally, the total resultant solution containing precipitates was transferred into a polytetrafluroethylene (PTFE)-lined stainless steel reaction vessel digestion bomb of 100ml capacity, Figure 1, then sealed and maintained at 150-200^oC for 5-16 hrs. After the hydrothermal process, the digestion bomb was cooled to ambient temperature naturally. The obtained precipitate was centrifuged, washed with double distilled water (DDW) for several times to remove the ions possibly remained in final products, and finally dried in vacuum at 100^oC in air. The dried powder was calcined at 400-500^oC for three hrs to obtain the nanorods or nanowires of MnO_2, NiO and ZnO.

3. Characterization

The structural properties of the synthesized nano-sized MnO_2, NiO and ZnO particles were measured by X-ray diffraction, Rigaku Japan (XRD) pattern with a CuK_α radiation (λ = 1.5406 Å) source. The XRD data were collected in 2θ range from 15°<2θ<80° by step-scanning 0.05° increments and scanning rate of 5°/min. Various microstructural features of MnO_2, NiO and ZnO powders were observed using scanning electron microscope (SEM, JSM-5910, LEO 4401). The sample for SEM observation was prepared by 10min ultrasonic dispersion of a small amount of sample in ethanol, drop of the solution was put onto aluminum stud, dried in air and then finally samples were coated with thin gold film.

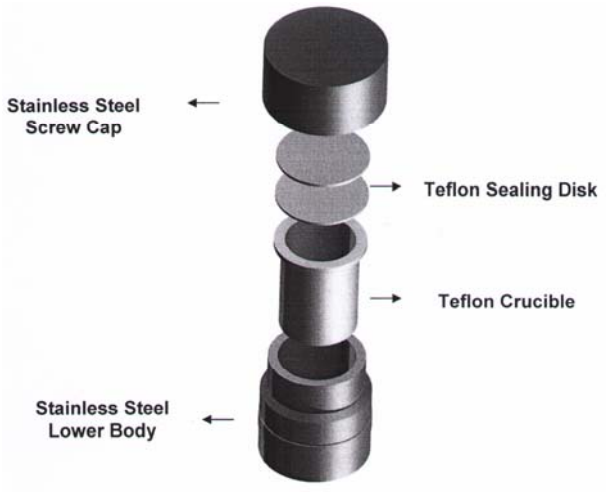

Figure 1. Stainless steel digestion bomb used for hydrothermal reactions.

The powder morphology of NiO was also observed by transmission electron microscopy, Jeol JEM 1010 Japan (TEM). The sample for TEM observation was prepared by dispersion of a small amount of sample in ethanol, drop of the solution was put onto carbon coated copper grid and dried in air. The chemical purity and stoichiometry of MnO_2, NiO and ZnO were measured by electron probe micro analyzer (EPMA) attached with SEM and inductively coupled plasma-optical emission spectrometer (ICP-OES, ARL 3580). The specific surface area of nanosized NiO and ZnO samples were determined by nitrogen adsorption and desorption isotherm Brunauer-Emmet-Teller (BET) technique at 77K [20]. The BET measurements were performed on ASAP 2010 Micrometrics instrument. The densities of powder samples were measured using Ultra-Pycnometer 1000 Quantachrome.

4. Results and Discussion

The synthesized powders of α-MnO_2, NiO and ZnO were brownish black, black and yellowish white respectively. The representative EPMA spectrum for ZnO is shown in Figure 2 which shows the presence of only zinc and oxygen as constitute elements in near stoichiometric ratio.

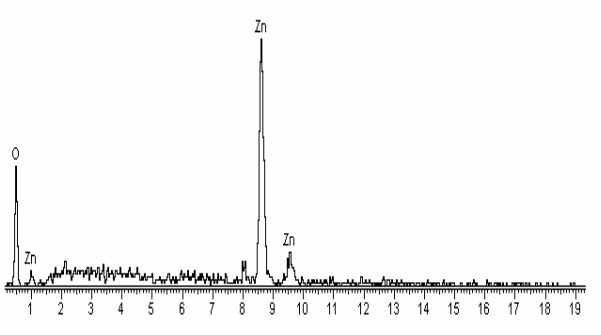

Figure 2. The representative EPMA spectrum for ZnO.

Figure 3 (a-c) show X-ray diffraction patterns of dried MnO_2, NiO and ZnO powders prepared by hydrothermal process. The diffraction peaks are fine, indicating the good crystalline nature (97%) of the products. In case of MnO_2 there is always a possibility of coexisting potassium ion in matrix arising from one of the starting materials used to prepare the manganese oxide. The XRD pattern of MnO_2, (Fig. 3a) did not show any characteristic peaks for impurities present in the sample indicating the high purity and good crystallinity of α-MnO_2. XRD data were analyzed with unit cell refinement and least squares programme (ITO and Celref V3 software) [21].The refined unit cell parameters, unit cell volume and symmetry of as-synthesized α-MnO_2, NiO and ZnO were measured and presented in Table 3. After refinement, the peak position and relative intensities of XRD pattern indicates that synthesized product is α-MnO_2 with cell parameters a = 9.784 Å, b = 9.784 Å, c = 2.795 Å, and unit cell volume is 267.53 $Å^3$. The d-spacing data shows that α-MnO_2 have body centered tetragonal crystal structure. These values were further confirmed with reported values JCPDS card (44-0141). The unit cell parameters were found close to the reported values [22]. All of indexed peaks (Fig. 3b) in the obtained XRD pattern are well matched with that of

bulk NiO JCPDS card (78-0423) which confirms that the synthesized NiO powder is crystalline and possesses a cubic structure. No peaks related to impurities were detected in XRD pattern [23]. The diffraction peaks in XRD pattern of ZnO, Fig.3c were indexed as hexagonal wurtzite structure, which were consistent with standard card JCPDS 36-1451. The sharp diffraction peaks indicate the good crystallinity of the synthesized product. The XRD study also indicate the strong preferred orientation is along the (101) direction [24].

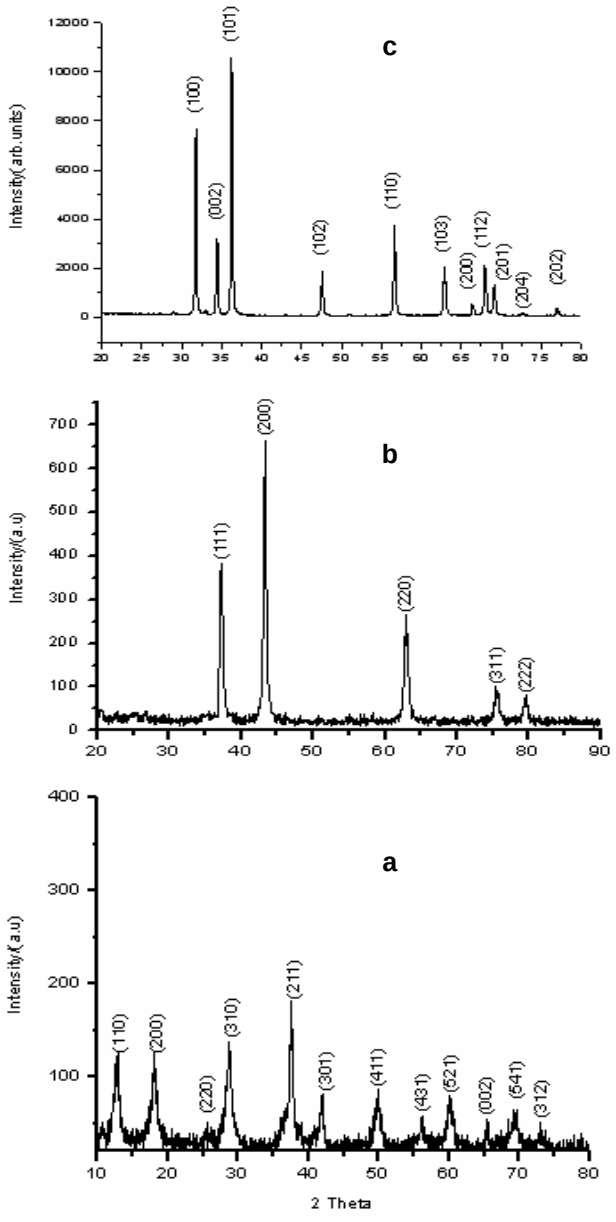

Figure 3 (a-c). XRD pattern of hydrothermally synthesized transition metal oxide nanocrystals, a. MnO_2, b. NiO and c. ZnO.

The average crystalline size (D) of the NiO and ZnO nanorods were estimated using the Debye-Scherrer formula [25],

$$D = \frac{0.89\,\lambda}{\beta \cos\theta} \quad (1)$$

Where D is the crystalline size (in nm), λ is the wavelength (in nm), ß the full width at half maximum (FWHM-in radian) intensity, and θ the Bragg diffraction angle (^{o}). The average crystalline size of NiO and ZnO nanorods were found 33 and 54 nm respectively.

The crystal growth mechanism of ZnO could be explained on the basis of following chemical reactions:

$$Zn(NO_3)_2.6H_2O + NaOH \rightarrow Zn(OH)_2 \rightarrow ZnO$$

In the presence of OH^{-1} ions in the solvent at high pH, temperature and pressure, $Zn(NO_3)_2.6H_2O$ dissociates to form $Zn(OH)_2$. Some times these $Zn(OH)_2$ might react with excess OH^{-1} ions to produce $[Zn(OH)_4]^{2-}$ ions. At high temperature these $Zn(OH)_2$ and $[Zn(OH)_4]^{2-}$ ions transform to ZnO crystals.

$$Zn(OH)_2 \rightarrow Zn^{2+} + 2OH^-$$

$$Zn^{2+} + 2OH^- \rightarrow ZnO + H_2O$$

These ZnO crystals agglomerate together to from hexagonal planer nucleus. At lower pH values, the presence of less amount of OH^{-1} causes the reaction to proceed much more slowly and hence initial nucleus get sufficient time to grow in both the lateral and longitudinal direction resulting in micro columns [26].

Different morphologies were observed by SEM and TEM for hydrothermally synthesized α-MnO_2, Nio and ZnO which are shown in Figure 4(a-e) taken at different magnifications. Fig. 4(a-b) revealed that α-MnO_2 sample consists of uniform nanowires with thickness ranging from 50-90nm and has a large aspect ratio. The morphology (Fig.4c) of NiO consists of nanobelts with ~80-120nm width ~20-40nm thickness and length lies in range of several microns. Further examinations of nanobelts were observed by TEM (Fig. 4d) which showed that NiO nanocrystals are looks like belts and grow in enormous length. The

morphology of ZnO consists of spike-type nanorods as shown in Fig. 4e. The diameters of the nanorods were in the range of 80-200 nm and lengths of 8 -12 μm. It was observed that nanorods. were originated from a single nucleation centre resulting into a large number of nanorod crystals with <100nm in diameters.

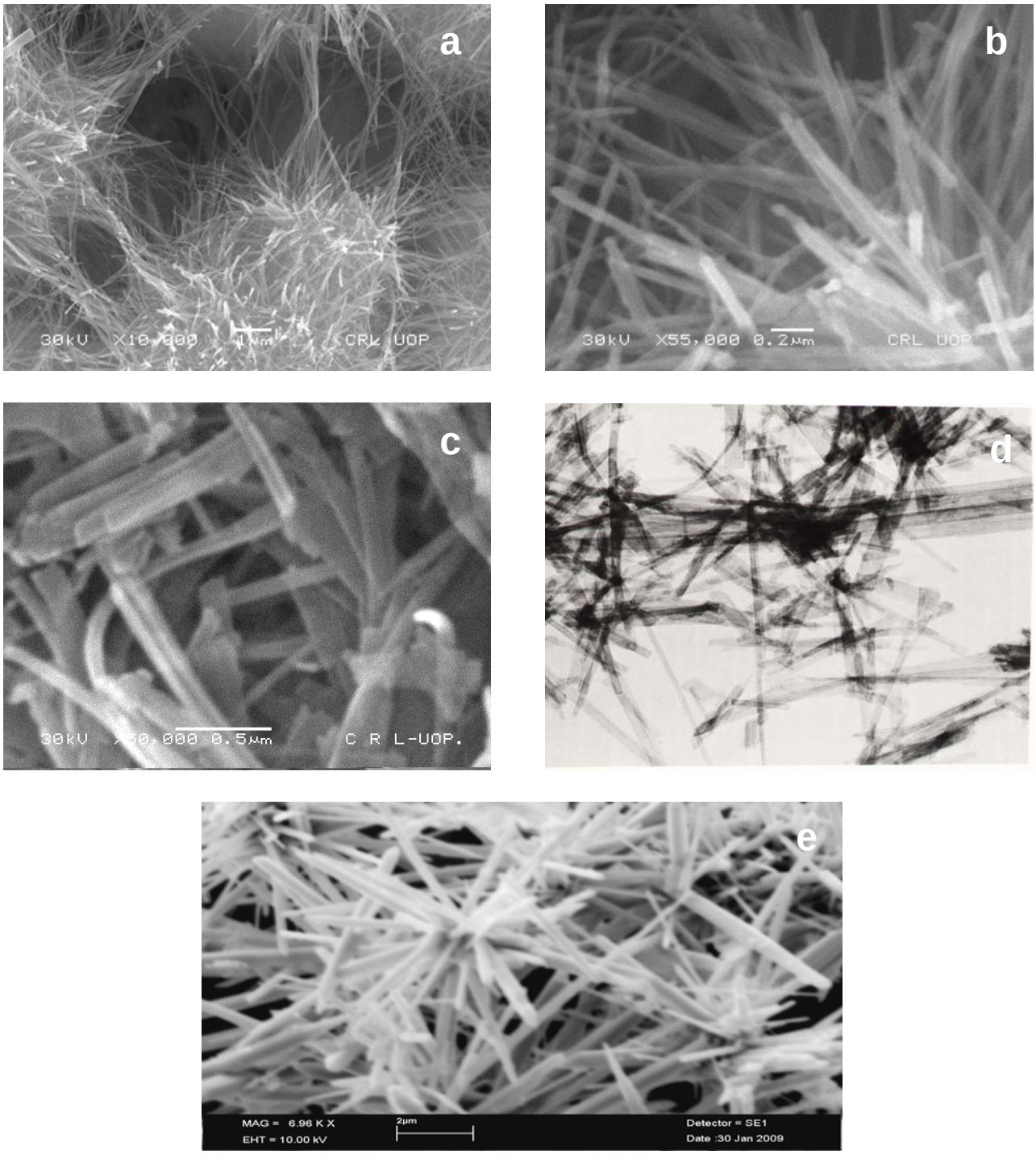

Figure 4 (a-e). SEM images of transition metal oxide nanocrystals, (a-b) nanowires of α-MnO_2, (c) nanobelts of NiO, (d) TEM image of NiO and (e), SEM image of nanorods of ZnO.

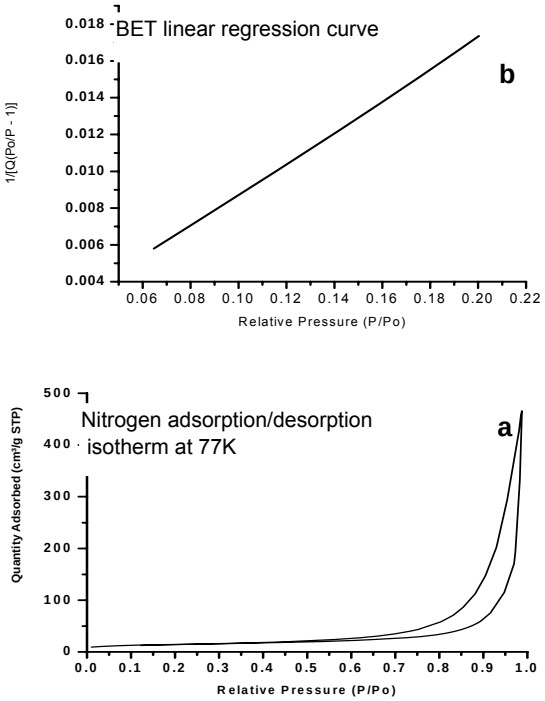

Figure 5 (a-b). Nitrogen adsorption and desorption isotherm of NiO nanocrystals, (a) Nitrogen adsorption/ desorption isotherm at 77K (b) BET curve.

Figure 5 (a-b) shows representative nitrogen absorption/desorption isotherm for NiO at 77 K (-196^{o}C). The isotherm (Fig. 5a) was analyzed for surface area using BET equations [27]. Regression analysis (Fig. 5b) shows that co-efficient of correction of BET straight line is ~ 0.992. The slope and intercept of the linearized form of the equation give the essential parameters used in determining the surface area. The BET surface areas and density values for nanosized NiO and ZnO powders are shown in Table 3. The BET surface area of nanosized ZnO and NIO were found 22.85m^2/g and 51.18m^2/g respectively.These values are in good agreement as reported values [28]. Surface area values of NiO and ZnO taken from BET model cannot be considered as truly representative of the actual surface area accessible to nitrogen sorption, due to the known shot-coming of model as applied to physio-sorption on microporous solids. For the reasons the nitrogen isotherms were analyzed for micropore area by t-plot method. The micropore area for nanosized NiO and ZnO samples were assessed by back extrapolation of the multilayer region of t-plot. The porosity of the nano oxide materials were calculated by the BJH method and the values of micropore area are also listed in Table 3. The specific surface area of nanosized powder measured by BET method at liquid nitrogen temperature and average grain size (crystalline size) was figured out according to the following equation [29]:

$$d_{BET} = \frac{6}{\rho S_{BET}} \times 10^{3} \quad (2)$$

Where d_{BET} is the crystalline size (nm), ρ is the density of nanosized powder (g/cm^3) estimated by pycnometer and S_{BET} is the BET specific surface area (m^2/g). In the present work the 58 nm of d_{BET} (crystalline size) of ZnO could be obtained by using 4.5 g/cm^3 powder density. On comparison of the results on the grain size determined by two methods, i.e., XRD and BET method. It was found that grain size estimated by BET surface area method was slightly higher than those of XRD. This was believed to be the results of agglomeration of the nanocrystalline powders owing to the high surface area and high surface energy of the ultrafine particles. The size determined by XRD was normally regarded as the size of the primary crystallites which could be denoted D, and the size deduced from the BET method by d_{BET} can be used as the size of the mean agglomerated particles. Thus, the ratio could be regarded as the mean agglomerated coefficient of the nanocrystals powders.The agglomeration coefficient was calculated using the following formula [29]:

$$C = \frac{d_{BET}}{D} \quad (3)$$

Where C is agglomeration coefficient, d_{BET}, D is the average crystalline size determined by BET and the XRD Scherrer formula, respectively. The inconsistency of ZnO crystalline size determined by BET methods and the XRD Scherrer formula indicated that there was agglomeration in the nano-sized ZnO powders. The agglomeration coefficient was found 1.08, which indicates that the agglo-meration was more evident in nanosized ZnO powder (Table 3).

Table 3. Physicochemical properties of some selected transition metal oxide nanocrystals (MnO_2, NiO and ZnO).

Physico-Chemical Analysis	*Nano Oxide Materials*		
	ZnO	NiO	*MnO_2*
Colour	Yellowish White	Black	*Brownish Black*
Density (g/cm^3)	4.51	5.34	---------
BET surface area (m²/g)	22.85	31.28	---------
BET crystalline size (nm)	58.22	35.92	--------
Agglomeration coefficient (C)	1.08	1.12	--------
t-plot micropore area (m²/g)	19.28	14.03	--------
XRD and SEM Analysis			
Debye-Scherrer crystalline size (nm)	54	32.30	*68.5*
Unit Cell Parameters			
a (Å)	3.249	4.175	*9.784*
b (Å)	3.249	4.175	*9.784*
c (Å)	5.205	4.175	*2.795*
Unit cell Volume (Å^3)	47.582	70.00	*267.53*
Symmetry	Hexagonal	Cubic	*Body centered tetragonal*
SEM (Morphology)	*Nanorods* *φ =80-200* *ω = 8-12*	*Nanobelts* *ξ = 80-120* *σ =20-40*	*Nanowires* *σ = 50-90nm*

φ = diameter(nm), ω = Length (μm), ξ = width (nm) and σ = Thichness (nm)

5. Conclusion

- A simple and cost effective hydrothermal method was successfully utilized to synthesize single phase crystalline α-MnO_2, NiO and ZnO nanowires, nanobelts and nanorods powder. The method neither requires complex apparatus and sophisticated techniques, catalysts nor the organic alkoxide templates.
- Crystalline α-MnO_2 nanowires were found to be (thickness = 50-90nm), NiO nanobelts (width = 80-120nm, thickness = 20-40nm) and ZnO nanowires (diameter=80-200nm, length=8-12μm).
- The structure development and morphology of selected α-MnO_2, NiO and ZnO nanocrystals were found influenced by hydrothermal parameters like pH, stoichiometric ratio, temperature and time.

Acknowledgements

One of authors (Yaqoob Khan, Ph.D Scholar) would like to appreciate the financial supports of Higher Education Commission (HEC), Government of Pakistan. Thanks due also to M. Masood, Dr. M. Bashir, M. Ashraf and Zahid Hussain for digestion bomb sketch, chemical analysis and XRD analysis respectively.

References

[1] P. Yang (Eds.), The Chemistry of nano-structured Materials, World Scientific Publishing Co. Inc., Singapore, (2003).

[2] A. S. Edelstein and R. S. Cammarata, Nano-materials: Synthesis, Properties, and Applications (Eds. Bristol, UK; Philadelphia, PA), Institute of Physics (1996).

[3] J. L. G. Fierro and L. L. G. Fierro, Metal Oxides: Chemistry and Applications, CRC Press, Taylor & Francis, Boca Raton (2005).

[4] G. Eranna, B. C. Joshi, D. P. Runthala and R. P. Gupta, Crit. Rev. Solid State Mater. Sci. **29** (2004) 111.

[5] T. R. Jow and J. P. Zheng, J. Electrochem. Soc. **145** (1998) 49.

[6] K. W. Nam and K. B. Kim, J. Electrochem. Soc. **149** (2002) A346.

[7] S. C. Pang and M.A. Anderson, J. Electrochem. Soc.**147** (2000) m444.

[8] M. S. Wu and H. H. Hsieh, Electrochimica Acta **53** (2008) 3427.

[9] C. M. Lieber, Solid State Common **107** (1998) 607.

[10] J. J. Wu, S.C. Liu, Adv. Mater. **15** (2003) 3294.

[11] D. W. Johnson, Jr., in Advances in Ceramics: Ceramic Powder Science; Vol. 21, pp. 3-19. American Ceramic Society (1987).

[12] L. P. Zhou, J. Xu, X.Q. Li and F. Wang, Mater. Chem. Phys. **97** (2006) 137.

[13] L. V. Hampden and M.J. Smith, Chemistry of Advanced Materials: An Overview; Wiley VCH: New York (1998).

[14] C. H. Lu and H. C. Wang, J. Eur. Ceram. Soc. **24** (2004) 717.

[15] P. He, X. Shen and H. Gao, J. Colloid Interface Sci. **284** *(*2005) 510.

[16] J. Kilier, C. J.Tucker, T.H. Kalantar and D. P. Green, Adv. Mater. **12** (2000) 1751.

[17] G. C. Ulmer and H. L. Barmes (eds.) Hydrothermal Experimental Techniques, John Wiley & Sons, New York (1981).

[18] S. K. Durrani, A. H. Qureshi, M.A. Hussain, M. Ahmad, N. Ahmed and N.K. Qazi, The Nucleus **46** (2009) 27.

[19] S.K. Durrani, J. Akhtar, N.A. Chughtai, M. Ahmed and M.J. Moughal, J. Mat. Sci. Tech., **21** (2005) 563.

[20] S. Brunauer, P.H. Emmett and E. Teller, J. Amer. Chem. Soc. **60** (1938) 309.

[21] J. W. Visser, J. App. Crystallogr. **2** (1969) 89.

[22] V. Subramanian, H. Zhu and B. Wei, J. Power Source **159** (2006) 361.

[23] X. Liu and S. Fu, Solid State Phenomena, **121** (2007) 1437.

[24] U. Alver, T. Kilinc, E. Bacaksiz, T. Kücükömeroğlu, S.Nezir, I.H.Mutlu, and F. Aslan, Thin Solid Films, **515** (2007) 3448.

[25] H. Klug and I. Alexander, X-ray Diffraction Procedures for Polycrystalline and Amorphous Materials, Wiley, New York (1974) p. 618.

[26] H. Kou, J. Wang, Y. Pan and J. Guo, Mat. Chem. Phys. **99** (2006) 325.

[27] P.J. M. Carrot and K.S.W. Sing, Chem. and Ind. (1986).

[28] H. M. Deng, J. Ding, Y. Shi, X. Y. Liu and J. Wang, J. Mater. Sci. **36** (2001) 3273.

[29] C.C. Chen, P. Liu and C. Lu, Chem. Eng. Journal. **144** (2008) 509.